

Engineering Extracellular Vesicles Restore the Impaired Cellular Uptake and Attenuate Intervertebral Disc Degeneration

Zhiwei Liao,[†] Hui Liu,[†] Liang Ma,[†] Jie Lei, Bide Tong, Gaocai Li, Wencan Ke, Kun Wang, Xiaobo Feng, Wenbin Hua,* Shuai Li,* and Cao Yang*



Cite This: <https://doi.org/10.1021/acsnano.1c04514>



Read Online

ACCESS |



Metrics & More



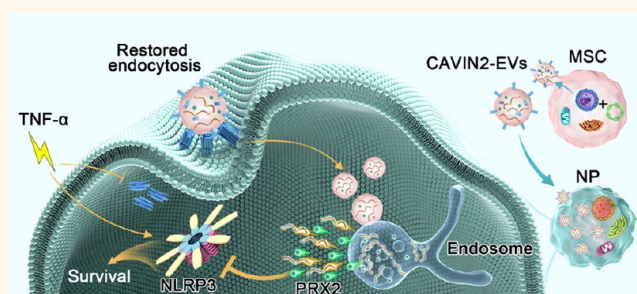
Article Recommendations



Supporting Information

ABSTRACT: Extracellular vesicles (EVs) are potential alternatives for mesenchymal stem cells (MSCs) in the treatment of musculoskeletal degenerative diseases, including intervertebral disc degeneration (IDD). Usually, EVs are internalized and then deliver bioactive molecules that impart phenotypic changes in recipient cells. For effective utilization of EVs in the IDD therapy, understanding the mechanism of EV uptake is of vital importance. In this study, we found that EVs delivered antioxidant proteins to protect against pyroptosis of nucleus pulposus cells (NPCs). In particular, the therapeutic effect of EVs decreased in TNF- α -treated NPCs due to the impaired caveolae-mediated endocytosis pathway. Transcriptome sequencing and functional verification revealed that caveolae associated protein 2 (Cavin-2) played an important role in the uptake process of EVs. We then constructed the Cavin-2-modified engineering EVs *via* the gene-editing of parental MSCs. These kinds of modified EVs presented an improved uptake rate in TNF- α -treated NPCs, which effectively ameliorated the cell death of NPCs in a three-dimensional hydrogel culture model and retarded the progression of IDD in the *ex vivo* organ culture model. Collectively, these findings illustrate the mechanism of EV uptake in NPCs and explore the application of engineering EVs in the treatment of IDD.

KEYWORDS: extracellular vesicles, mesenchymal stem cells, intervertebral disc degeneration, endocytosis, organ culture



INTRODUCTION

Low back pain (LBP) is a major public health burden, and its cost is increasing rapidly with an aging population.¹ LBP is closely relevant to intervertebral disc degeneration (IDD) diseases, which belong to degenerative changes in the musculoskeletal system.² IDD is characterized by the loss of resident cells and extracellular matrix.³ As the major cell type in the center of the intervertebral disc, nucleus pulposus cells (NPCs) produce an extracellular matrix and maintain the balance of the disc microenvironment.^{3,4} Injury and dysfunction of NPCs plays a detrimental role in the progression of IDD.⁵ Therapeutic treatment on impaired NPCs presents a promising way for retarding IDD.

Currently, IDD-associated back pain is commonly treated with conservative ways or invasive surgical procedures as the last choice.⁵ Experimental treatment based on mesenchymal stem cell (MSC) therapy, combined or not with biomaterials, provides a potential method for intervertebral disc regeneration.³ Extracellular vesicles (EVs) inherit the merits from their parental MSCs, which could regulate inflammation and

immune response, as well as exert a proliferative and antioxidative effect.⁶ Among these EVs, small extracellular vesicles are nanosized particles with the size between 30 and 150 nm that contain various bioactive molecules and deliver cargoes in cell-to-cell communication.⁶ MSC-derived small EVs gradually become an alternative treatment used in regenerative therapy for degenerative diseases.^{7,8} Our previous studies have shown that MSC-derived small EVs could suppress advanced glycation end-product-induced apoptosis of NPCs *in vitro* and *in vivo*.⁹ However, the therapeutic effect of MSC-derived EVs on impaired NPCs during the IDD has not been fully investigated.

Received: May 27, 2021

Accepted: August 31, 2021

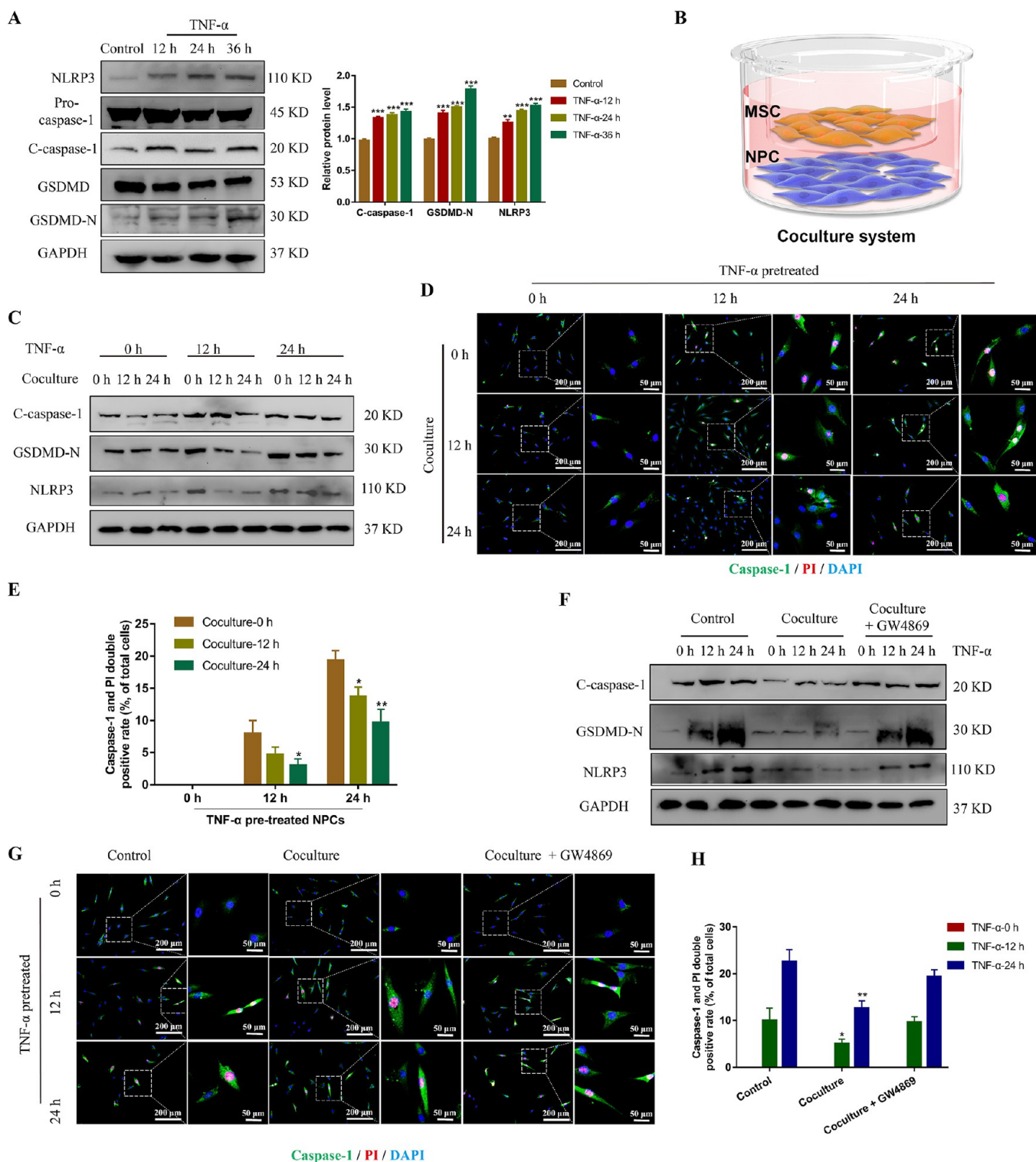


Figure 1. MSC coculture attenuates TNF- α -induced NPC pyroptosis. (A) NPCs were treated with 50 ng/mL TNF- α at different time periods. Western blot and quantification analysis of NLRP3, pro-caspase-1, C-caspase-1, GSDMD, and GSDMD-N. * $P < 0.05$, ** $P < 0.01$, *** $P < 0.001$ vs control group. (B) Schematic graph of NPC coculture with MSCs. NPC, nucleus pulposus cell; MSC, mesenchymal stem cell. (C) NPCs were cocultured with or without MSCs for different times. Western blot analysis of NLRP3, C-caspase-1, and GSDMD-N. (D,E) Immunofluorescence analysis of caspase-1 and PI (D) and quantification of double-positive cell rate (E) in NPC coculture with or without MSCs. * $P < 0.05$, ** $P < 0.01$, *** $P < 0.001$ vs corresponding coculture-0h group. (F) NPCs were cocultured with MSCs and cotreated with or without GW4869 (20 μ m, 24 h). Western blot analysis of NLRP3, C-caspase-1, and GSDMD-N. (G,H) Immunofluorescence analysis of caspase-1 and PI (G) and quantification of double-positive cell rate (H). The dashed boxes mark the enlarged region of interest. * $P < 0.05$, ** $P < 0.01$, *** $P < 0.001$ vs corresponding control group. Data are presented as the mean \pm SD, $n = 3$.

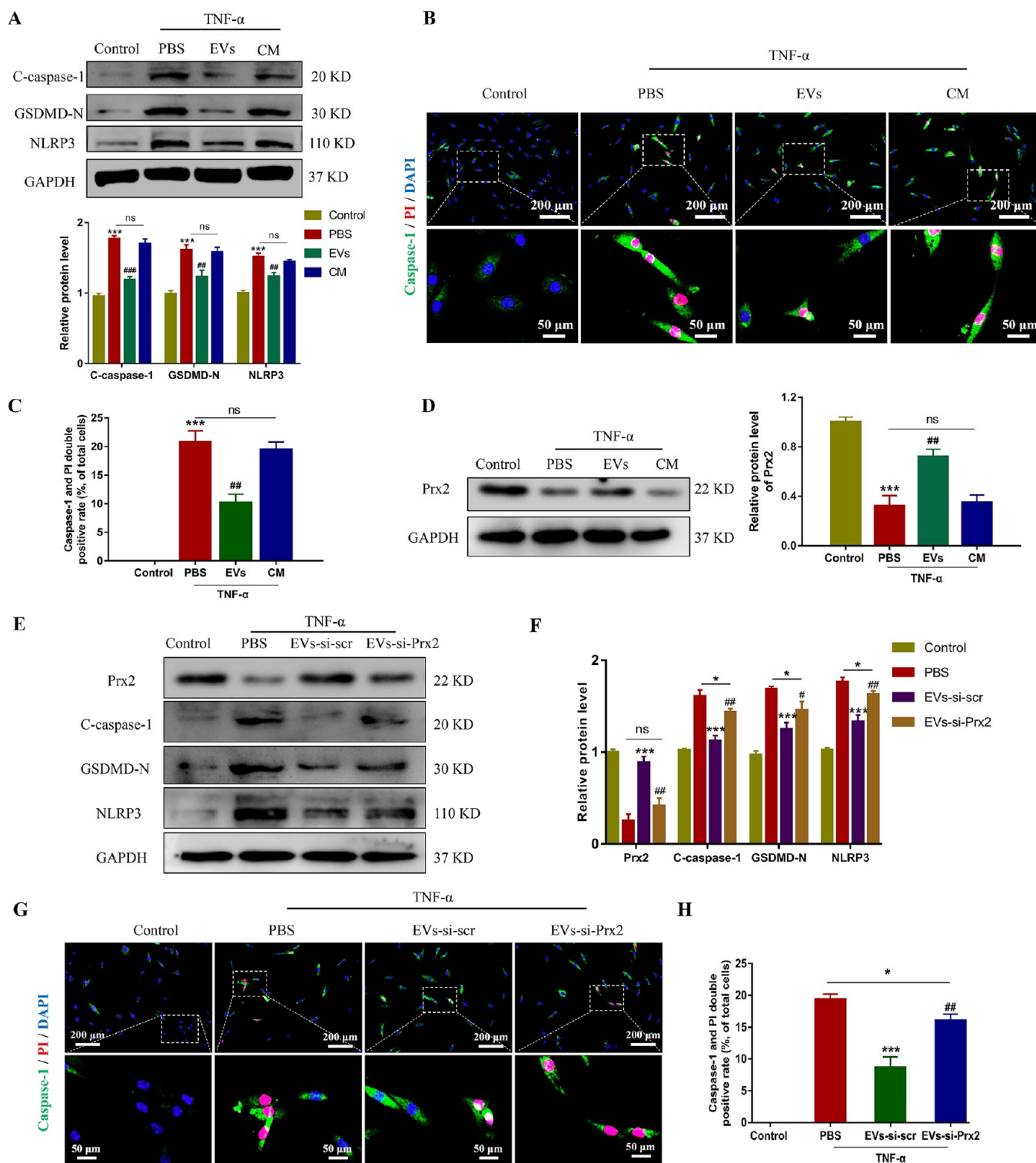


Figure 2. EVs deliver peroxiredoxin-2 to protect against pyroptotic NPC death. (A) TNF- α -pretreated NPCs were incubated with PBS, EVs (100 μ g/mL), or culture medium depleted with EVs (CM) for 24 h. NPCs treated without TNF- α were used as the control. Western blot analysis and quantification of NLRP3, C-caspase-1, and GSDMD-N. (B,C) Immunofluorescence analysis of caspase-1 and PI (B) and quantification of double-positive cell rate (C) in PBS, EVs, or CM-treated NPCs. (D) Peroxiredoxin-2 (Prx2) protein level in NPCs incubated with PBS, EVs, or CM for 24 h. * $P < 0.05$, ** $P < 0.01$, *** $P < 0.001$ vs control group. # $P < 0.05$, ## $P < 0.01$, ### $P < 0.001$ vs PBS group; ns, not significant. (E,F) NPCs were incubated with EVs-si-scr (EVs from MSCs treated with si-scr, 100 μ g/mL) or EVs-si-Prx2 (EVs from MSCs treated with si-Prx2, 100 μ g/mL) for 24 h. Protein levels of Prx2, C-caspase-1, GSDMD-N, and NLRP3. (G,H) Immunofluorescence analysis of caspase-1 and PI (G) and quantification of double-positive cell rate (H). The dashed boxes mark the enlarged region of interest. * $P < 0.05$, ** $P < 0.01$, *** $P < 0.001$ vs PBS group. # $P < 0.05$, ## $P < 0.01$, ### $P < 0.001$ vs EVs-si-scr group; ns, not significant. Data are presented as the mean \pm SD, $n = 3$.

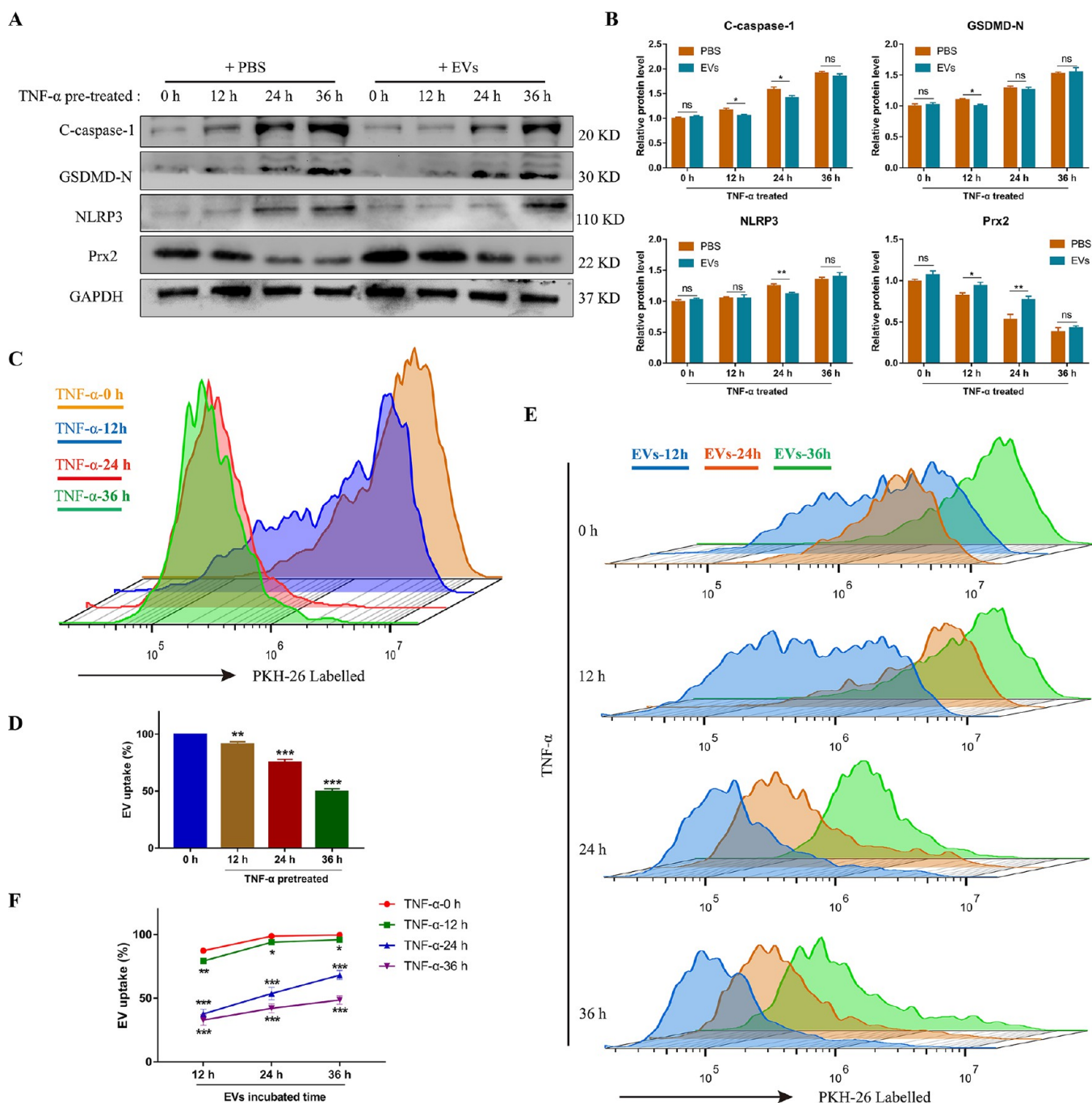


Figure 3. TNF- α impairs the EV uptake in NPCs. (A,B) TNF- α -pretreated NPCs were incubated with PBS or EVs (100 μ g/mL) for 24 h. Western blot (A) and quantification analysis (B) of NLRP3, C-caspase-1, GSDMD-N, and Prx2. * P < 0.05, ** P < 0.01, *** P < 0.001 vs corresponding PBS group. (C,D) Flow cytometry of TNF- α -pretreated NPCs incubated with PKH26-labeled EVs for 24 h (C) and the relative EV uptake based on flow cytometry analysis (D). * P < 0.05, ** P < 0.01, *** P < 0.001 vs TNF- α -pretreated-0h group. (E,F) Flow cytometry of TNF- α -pretreated NPCs incubated with PKH26-labeled EVs for 12, 24, or 36 h (E) and relative EV uptake rates based on flow cytometry analysis (F). * P < 0.05, ** P < 0.01, *** P < 0.001 vs corresponding TNF- α -pretreated-0h group. Data are presented as the mean \pm SD, n = 3.

Usually, EVs are identified and internalized by recipient cells and then complete the mission of protein or RNA delivery.¹⁰ Recipient cells accept exogenous EVs mainly *via* an endocytosis route, while the mechanisms for which EVs are engulfed by NPCs are unknown.^{11,12} Pinocytosis is a type of endocytosis that involves cellular uptake of small particles (size <1 μ m), which includes clathrin-mediated endocytosis, caveolae/lipid raft-dependent endocytosis, macropinocytosis,

or other still poorly characterized mechanisms.^{13,14} To realize an effective utilization of EVs in IDD therapy, understanding the underlying endocytic mechanism of EV uptake is of vital importance.

Inflammasome activation has been confirmed to play an essential role in the pathogenesis of IDD.¹⁵ During the progression of IDD, the nod-like receptor protein 3 (NLRP3) inflammasome activates gradually and elicits the cleavage of

caspase-1 and secretion of IL-1 β , which could cause cell damage if uncontrolled.¹⁶ Gasdermin D (GSDMD) is a substrate of caspase-1 that mediates pyroptotic cell death.¹⁷ GSDMD-mediated pyroptosis plays a detrimental role in IDD, and intervention on cell pyroptosis protects against the progression of IDD.^{18,19} Some studies have revealed that both the microenvironment around the recipient cells and cell functional state affect the uptake of EVs.^{20,21} Since inflammasome activation and pyroptosis are involved in cell injury and IDD progression, the inflammatory microenvironment affects the NPCs' function and may alter the efficiency of EVs' uptake.

In this study, we found that MSCs ameliorate the inflammasome activation and NPC pyroptosis through the paracrine effect primarily mediated by EVs delivery. In particular, peroxiredoxin-2 (Prx2) in EVs protected against pyroptotic NPC death, while this effect was weakened in TNF- α -impaired NPCs. Therefore, we suspected that the efficiency of EV uptake is decreased in impaired NPCs, which may account for EV treatment failure. Based on the application of an endocytosis inhibitor and RNA sequencing analysis, it was indicated that the uptake of EVs is mainly mediated by a caveolae-dependent endocytosis pathway. Administration of engineering EVs with caveolae-associated protein 2 (Cavin-2) expression restored the therapeutic effect on NPCs. Moreover, impaired NPCs showed a repaired uptake efficiency of modified EVs in a three-dimensional (3-D) hydrogel system. These modified EVs also presented regenerative potentials in the *ex vivo* disc degeneration model. Our investigations offer insights into the therapeutic mechanism of EVs in IDD, with practical implications for MSC-based intervertebral disc regeneration.

RESULTS AND DISCUSSION

MSC Coculture System Ameliorates the Pyroptotic Death of TNF- α -Treated NPCs. Pro-inflammatory cytokines contribute greatly to the progression of IDD.²² Here, we utilized different doses of TNF- α -treated NPCs at different time periods, and the cell viability was assessed (Figure S1A,B). TNF- α treatment increased the expression of pyroptosis-related proteins, including cleaved caspase-1 (C-caspase-1) and N-terminal of GSDMD (GSDMD-N) and NLRP3 in NPCs in a time-dependent manner (Figure 1A). The rate of caspase-1 and propidium iodide (PI) double-positive cells, which stands for pyroptotic death, was also increased in TNF- α -treated NPCs in a time-dependent manner (Figure S1C,D). To investigate the therapeutic effects of MSCs on NPCs, we constructed a coculture model with cell-to-cell indirect contact (Figure 1B). Coculture with MSCs significantly decreased the expression of C-caspase-1, GSDMD-N, and NLRP3 in NPCs, and this therapeutic effect was more evident as the coculture time increased (Figure 1C and Figure S1E–G). The rate of pyroptotic death also decreased in the MSC coculture group (Figure 1D,E). In this coculture model, the therapeutic effect was most likely mediated by MSCs' paracrine effect. EVs are representative portion of MSCs' secretome and mediate the paracrine effects of parent cells.²³ Then, we used the specific inhibitor of EV secretion, GW4869 in MSCs. We found that GW4869 treatment abrogated the therapeutic effect of MSCs' coculture in NPCs (Figure 1F and Figure S1H–J). Immunofluorescence analysis also supported that GW4869 treatment increased the pyroptotic NPC death rate in the coculture group (Figure 1G,H). These results

demonstrated that secretory EVs may mediate the therapeutic effects of MSC coculture, while the underlying mechanism needs further investigation.

MSC-Derived EVs Protects against TNF- α -Induced NPCs Pyroptosis. In order to confirm the effects of EVs, EVs were isolated from MSC culture medium and then incubated with NPCs. Compared with NPCs incubated with PBS or EV-depleted culture medium (CM), the EV fraction reduced the expression of C-caspase-1, GSDMD-N, and NLRP3 in TNF- α -treated NPCs (Figure 2A). Incubation with EVs significantly decreased the pyroptotic death rate of NPCs (Figure 2B,C). Several studies have reported the relationship between peroxiredoxin proteins and inflammation regulation.^{24–26} Based on our previous proteomics data of small EVs,²⁷ we found that peroxiredoxin-2 (Prx2) is abundant in MSC-derived EVs (Figure S2A,B). Then, we detected the level of Prx2 in EVs and CM and found that Prx2 was enriched in the EV fraction (Figure S2C). Moreover, the expression level of Prx2 was decreased in TNF- α -treated NPCs but significantly increased when incubated with EVs, indicating the delivery of Prx2 to NPCs (Figure 2D).

To further confirm the role of Prx2 in EVs, we isolated EVs from MSCs transfected with PRDX2 (encodes peroxiredoxin-2)-siRNA (EVs-si-Prx2) or a scrambled siRNA (EVs-si-scr), and the transfection efficiency was assessed in MSCs (Figure S2D). Then, we measured the Prx2 level in these EVs, and EVs-si-Prx2 had a low level of Prx2 (Figure S2E). Moreover, the expressions of C-caspase-1, GSDMD-N, and NLRP3 were at levels in the EVs-si-Prx2 group higher than those in the EVs-si-scr group (Figure 2E,F). Immunofluorescence analysis also revealed that the pyroptotic NPC death was increased in the EVs-si-Prx2-treated NPC group (Figure 2G,H). These results showed that Prx2 plays a role in the EV-mediated therapeutic effect, and the decreased level of Prx2 in EVs partly impairs the therapeutic efficacy on NPCs.

Impaired Uptake of EVs in NPCs Decreases the Therapeutic Efficacy. We investigated the effects of EVs on NPCs in different status. NPCs were pretreated with TNF- α and then incubated with EVs. We found that EV incubation has little influence on the expression levels of pyroptosis-related proteins in TNF- α -pretreated-36h NPCs (Figure 3A,B). It was indicated that EVs present decreased therapeutic potentials on TNF- α -pretreated NPCs. We assumed that the EV uptake was impaired in TNF- α -treated NPCs. Then, EVs were labeled with fluorescent dye PKH-26 and incubated with NPCs. Immunofluorescence analysis revealed that the mean fluorescence intensity in the TNF- α -24h and TNF- α -36h group was much lower than that in the TNF- α -0h group (Figure S3A,B). Flow cytometry also supported that the rates of labeled NPCs were decreased in the TNF- α -24h and TNF- α -36h groups, indicating the impairment of EV uptake (Figure 3C,D). To further confirm our results, the EV incubation time was prolonged and the EV uptake efficiency was evaluated. TNF- α -pretreated NPCs presented an increased EV uptake rate with incubation time extended, while the maximum rate was still lower than the TNF- α -untreated NPCs (Figure 3E,F). The variation profile of EV uptake in immunofluorescence was consistent with the results calculated by flow cytometry (Figure S3C,D). These discoveries demonstrated that TNF- α treatment impairs the EV uptake, resulting in a decline of EVs' therapeutic efficiency on NPC pyroptosis.

Cellular Uptake of EVs Is Mediated by Caveolae-Dependent Endocytosis. To clarify the mechanism of EVs

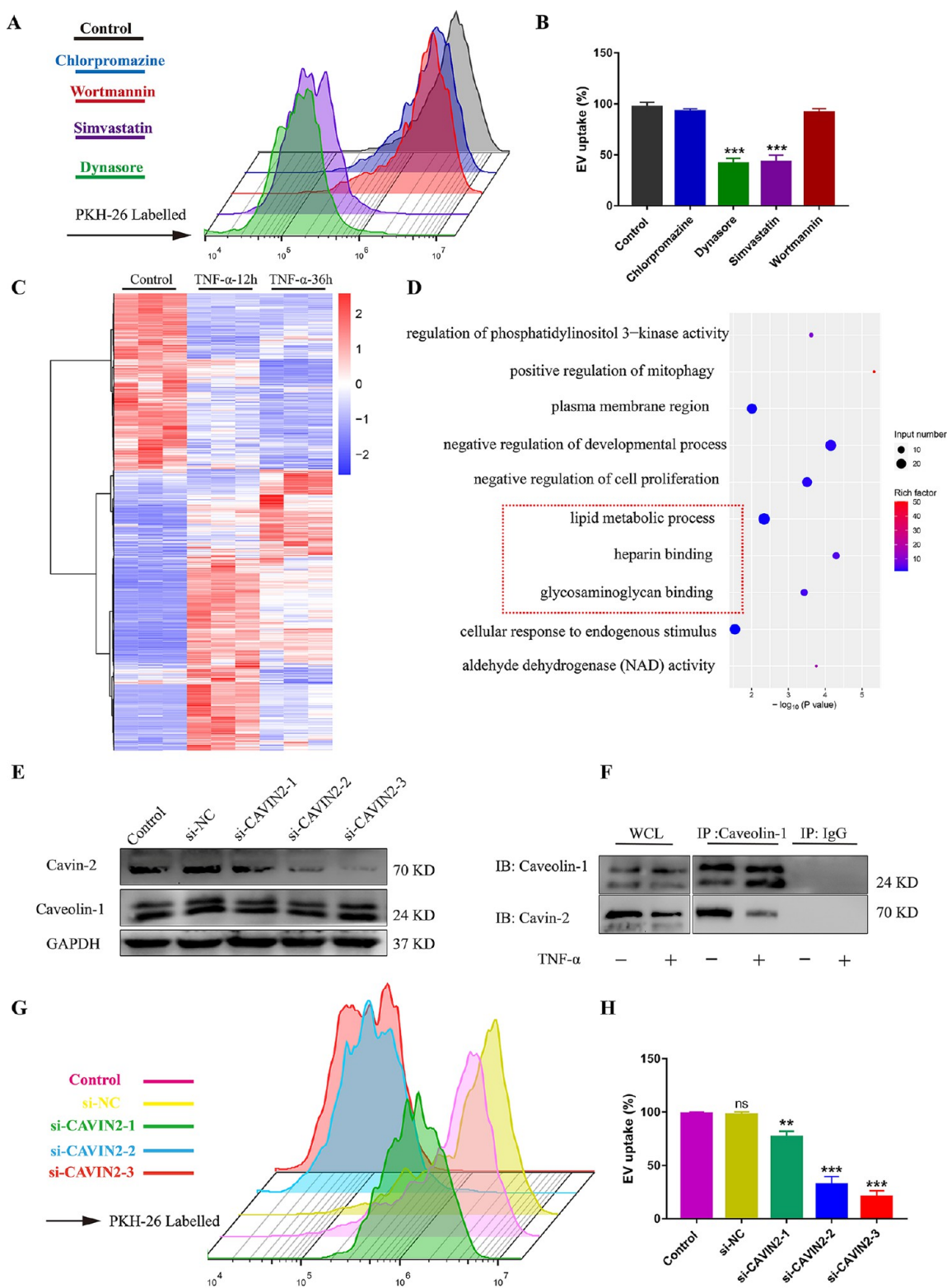


Figure 4. Cavin-2 plays a role in the caveolae-associated EV uptake pathway. (A,B) Flow cytometry of inhibitor-pretreated NPCs incubated with PKH26-labeled EVs for 24 h (A) and relative EVs uptake rate (B) (application information on inhibitors: chlorpromazine, 100 μ M, 6 h; wortmannin, 50 nM, 24 h; Dynasore, 50 μ M, 6 h; simvastatin, 20 μ M, 12 h). * P < 0.05, ** P < 0.01, *** P < 0.001 vs control group. (C) Heatmap of cluster analysis of the differentially expressed genes in the TNF- α -treated-36h and TNF- α -treated-12h groups compared to the control group (TNF- α -treated-0h). (D) Bubble diagram of GO enrichment analysis of the 188 differentially down-expressed genes. (E) NPCs were transfected with three kinds of CAVIN2 siRNAs. Protein levels of Cavin-2 and caveolin-1 were measured. (F) Immunoprecipitation analysis of caveolin-1 and Cavin-2 in NPCs. WCL, whole cell lysates. IgG was used as a negative control. (G,H) Flow cytometry of si-CAVIN2-transfected NPCs incubated with PKH26-labeled EVs for 24 h (G) and relative EVs uptake rates (H). * P < 0.05, ** P < 0.01, *** P < 0.001 vs control group; ns, not significant. Data are presented as the mean \pm SD, n = 3.

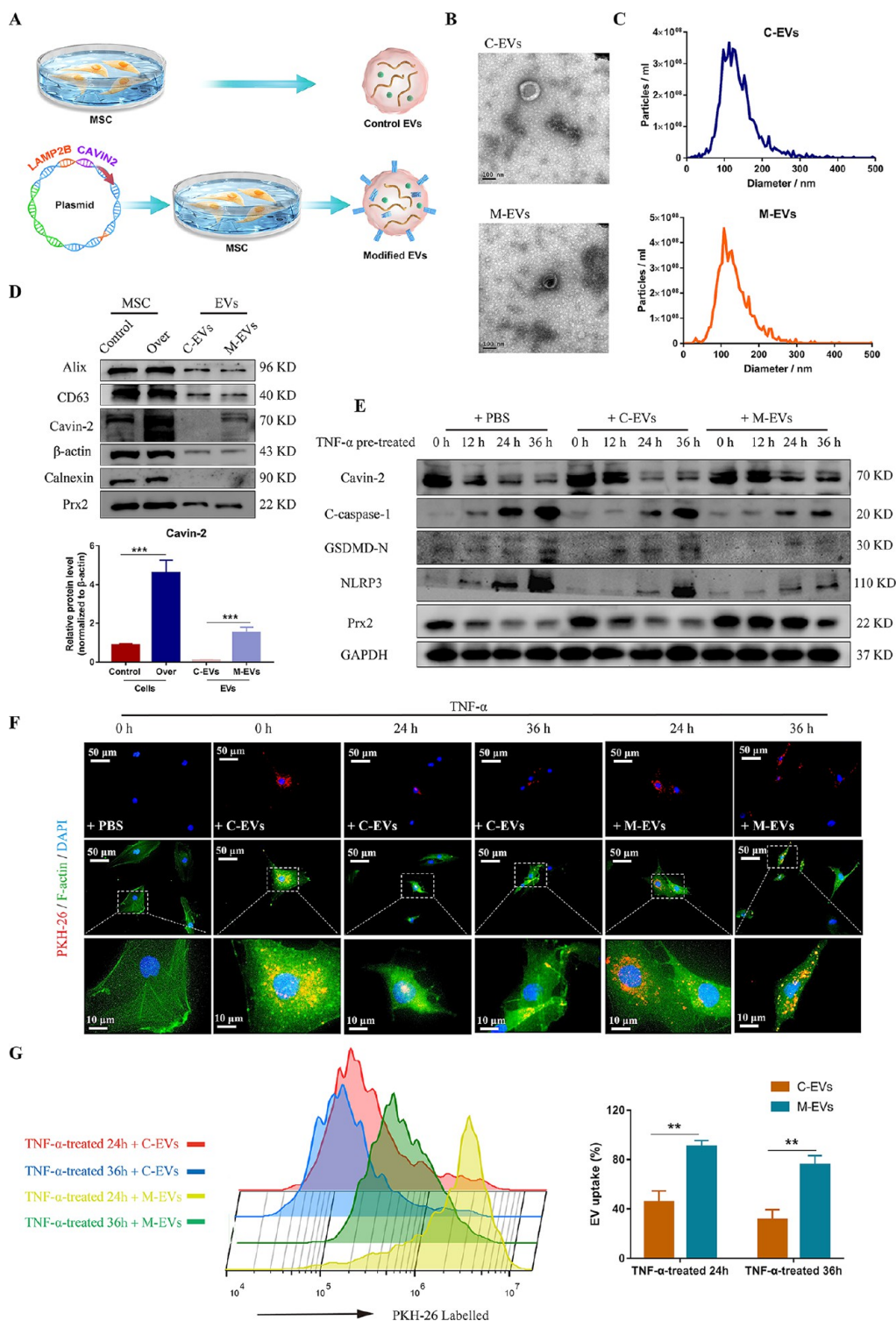


Figure 5. Cavin-2-modified engineering EVs restore the EV uptake in the impaired NPCs. (A) Schematic graph of the preparation workflow for engineering EVs. Cavin-2, caveolae-associated protein 2; MSC, mesenchymal stem cell; EVs, extracellular vesicles. (B,C) Transmission electron microscopy images and nanoparticle tracking analysis results of C-EVs (control EVs from normal MSCs) and M-EVs (modified EVs from Cavin-2-engineered MSCs). (D) Protein levels of Cavin-2, Prx2, CD63, Alix, β -actin, and Calnexin in MSCs and EV fraction (top panel). Quantification of Cavin-2 levels in MSCs and EV fraction (bottom panel). β -Actin was a loading control, and Calnexin was a negative control of EVs. * $P < 0.05$, ** $P < 0.01$, *** $P < 0.001$ vs control group or C-EVs group. (E) TNF- α -pretreated NPCs were incubated with PBS, C-EVs (100 $\mu\text{g}/\text{mL}$), or M-EVs (100 $\mu\text{g}/\text{mL}$) for 24 h. Western blot analysis of Cavin-2, NLRP3, C-caspase-1, GSDMD-N, and Prx2. (F) NPCs were pretreated with TNF- α for different time periods and then incubated with PBS, C-EVs, or M-EVs. Immunofluorescence analysis showed the internalization of PKH26-labeled (red) EVs in these groups. The dashed boxes mark the enlarged area which show the distribution of PKH-labeled EVs in the single cell. (G) Flow cytometry of TNF- α -pretreated NPCs incubated with PKH26-labeled EVs for 24 h and relative EV uptake rates. * $P < 0.05$, ** $P < 0.01$, *** $P < 0.001$ vs corresponding C-EV group. Data are presented as the mean \pm SD, $n = 3$.

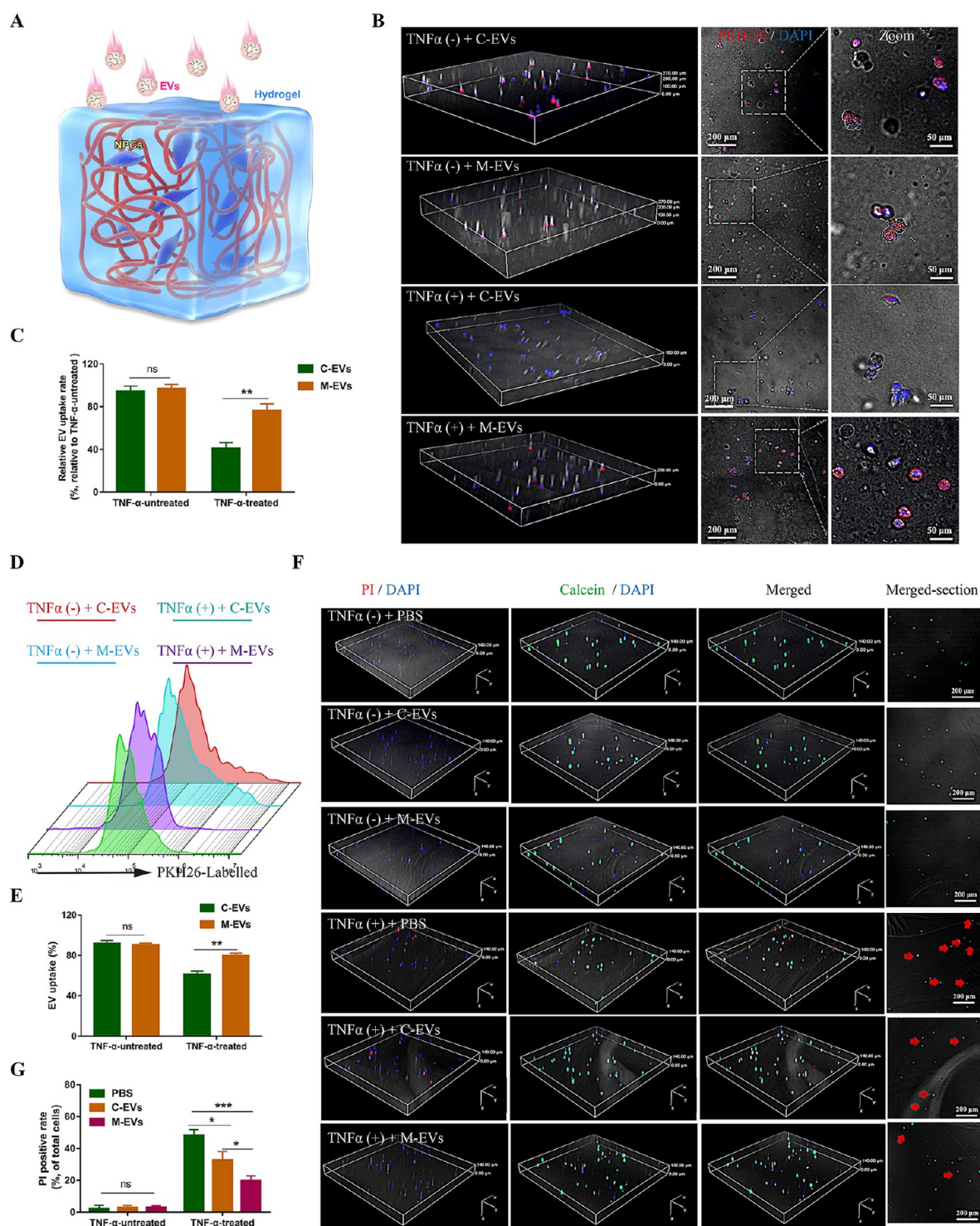


Figure 6. Internalization assay and therapeutic effects of EVs in a 3-D hydrogel model. (A) Schematic graph of NPCs incubated with C-EVs (control EVs) or M-EVs (modified EVs) in a 3-D hydrogel. EVs, extracellular vesicles; NPCs, nucleus pulposus cells. (B,C) Confocal fluorescent images (B) showed the internalization of PKH26-labeled EVs in NPCs with or without TNF- α treatment (50 ng/mL, 24 h) at stereoscopic and transverse sectional levels. The dashed boxes mark the enlarged region of interest. Relative EV uptake rates based on the fluorescence intensity (C). (D,E) Flow cytometry of NPCs incubated with C-EVs (100 μ g/mL) or M-EVs (100 μ g/mL) for 24 h in a hydrogel model (D) and relative EV uptake rates (E). * $P < 0.05$, ** $P < 0.01$, *** $P < 0.001$ vs corresponding C-EV group; ns, not significant. (F,G) Live/dead staining in the 3-D hydrogel model at stereoscopic and transverse sectional levels (F). Red arrows indicated the PI staining cells. Corresponding quantification analysis of PI-positive cell rates (G). * $P < 0.05$, ** $P < 0.01$, *** $P < 0.001$ vs corresponding PBS group; ns, not significant. Data are presented as the mean \pm SD, $n = 3$.

uptake, different inhibitors for endocytosis pathway were used in treating NPCs. Both chlorpromazine, which blocks clathrin-mediated endocytosis, and wortmannin, an inhibitor of the

phosphoinositide 3-kinase, had little effect on the EV uptake (Figure 4A,B). However, the dynamin inhibitor, dynasore, and simvastatin, which is involved in cholesterol synthesis, could

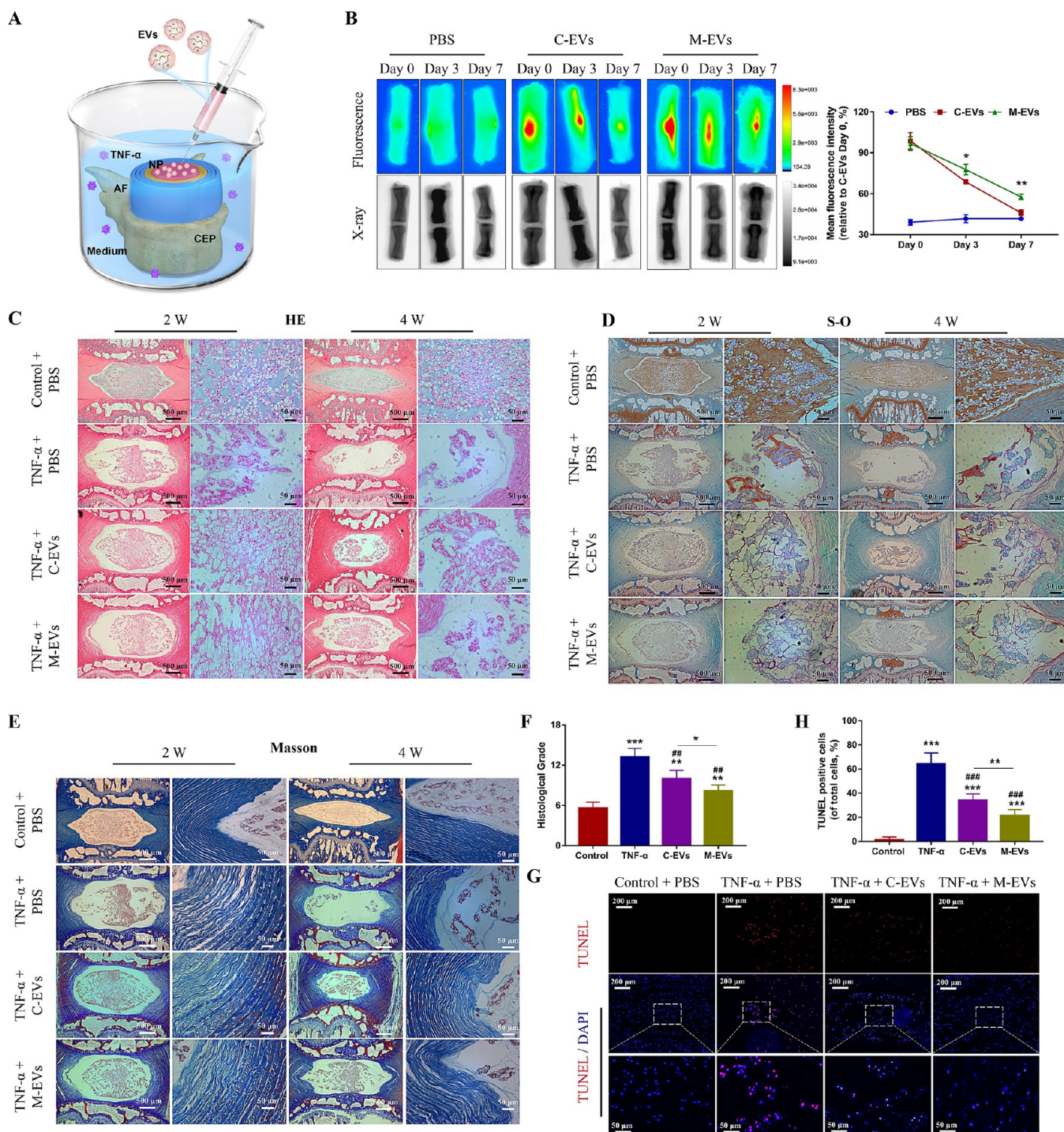


Figure 7. Utilization of EVs in an *ex vivo* disc culture model. (A) Schematic graph of isolated disc organ culture model with C-EV (control EVs) or M-EV (modified EVs) administration. EVs, extracellular vesicles; NP, nucleus pulposus; AF, annulus fibrosus; CEP, cartilaginous end plate; TNF- α , tumor necrosis factor α . (B) *Ex vivo* imaging and corresponding quantification analysis showed the fluorescence intensity after the delivery of Dil-labeled C-EVs or M-EVs (100 μ g/mL, 2 μ L) into the disc at day 0, day 3, and day 7. * P < 0.05, ** P < 0.01, *** P < 0.001 vs corresponding C-EV group. (C–E) Histological analysis including HE, S-O, and Masson staining showed the morphology of disc organ treated with PBS, C-EVs, or M-EVs. Medium with TNF- α was used to induce disc degeneration. (F) Histological grades based on the degenerative scale of discs in the different groups. (G,H) TUNEL analysis (G) and corresponding quantification (H) of TUNEL-positive cell rates revealed the condition about cell apoptosis in the different groups. * P < 0.05, ** P < 0.01, *** P < 0.001 vs control group. # P < 0.05, ## P < 0.01, ### P < 0.001 vs TNF- α group. Data are presented as the mean \pm SD, n = 5.

significantly decrease the EV uptake in NPCs (Figure 4A,B). It was speculated that caveolae/lipid raft-dependent endocytosis may be involved in EV internalization. Then we conducted RNA sequencing to analyze the gene expression in TNF- α -

treated NPCs (Figure 4C). We found that 326 genes up-expressed and 188 genes down-expressed both in TNF- α -treated-12h and TNF- α -treated-36h groups (vs the 0h group) (Figure S4A). GO and KEGG enrichment analysis of

differentially up-expressed genes showed the activation of inflammatory-related signaling (Figure S4C). GO enrichment analysis revealed that differentially down-expressed genes were related with lipid metabolic process, heparin and glycosaminoglycan binding (Figure 4D).

Among these genes, one significantly down-expressed gene, CAVIN2 (encodes Cavin-2, also known as SDPR), was involved in caveolae-mediated endocytosis. Previous study has shown that Cavin-2 binds to caveolin-1 and induces the formation of plasma membrane curvature, which mediates the endocytosis of extracellular cargoes.²⁸ We then measured the expression level of proteins which engaged in caveolae-mediated endocytosis, including caveolins (caveolin-1, caveolin-3) and caveolae-associated proteins (Cavin-1, Cavin-2, and Cavin-3). The expression of Cavin-2 significantly decreased in TNF- α -treated NPCs (Figure S4D,E). Immunoprecipitation analysis revealed that Cavin-2 binds to caveolin-1 in NPCs (Figure 4F). Then, three CAVIN2-siRNAs were used to knockdown the expression of Cavin-2 in NPCs (Figure 4E and Figure S4F). It was indicated that Cavin-2 knockdown significantly reduced the EV uptake (Figure 4G,H). These results showed that the EV uptake in NPCs is mediated by caveolae-dependent endocytosis, and Cavin-2 plays a critical role in this process.

Cavin-2-Engineered EVs Reacquire a Therapeutic Effect on Impaired NPCs. In order to repair the endocytosis pathway of NPCs, we designed modified EVs using a gene-editing technique. We constructed Cavin-2 expression vectors and transfected them into MSCs (Figure 5A). As Lamp2b proteins are located in the EV membrane, it could be predicated that EVs with the fusion expression of Cavin-2 and Lamp2b express Cavin-2 in their membrane.²⁹ Then, we isolated EVs from the control MSCs (C-EVs) and from the cavin2-transfected MSCs (M-EVs). Analysis of EV morphology and size showed no significant difference between C-EVs and M-EVs (Figure 5B,C). The protein levels of Cavin-2 in cells and EV fraction were measured by Western blot, indicating that Cavin-2 was robustly expressed in M-EVs (Figure 5D). To evaluate the effects of C-EVs and M-EVs on NPCs, the levels of pyroptosis-related proteins were measured in TNF- α -pretreated NPCs (Figure 5E). In particular, the administration of M-EVs significantly decreased the levels of pyroptosis-related proteins in TNF- α -pretreated-36h NPCs compared with the C-EV group (Figure 5S A–E). To further assess the differences of EV endocytosis in NPCs, we labeled the EVs with PKH-26 and compared the intracellular fluorescence intensity in NPCs (Figure 5F). The uptake amounts of M-EVs in TNF- α -pretreated NPCs were higher compared to those in the C-EVs group (Figure 5S F). The EV uptake rate based on the cytometry analysis in the M-EV group was higher than that in the C-EV group (Figure 5G). These results revealed that Cavin-2 engineering EVs restore the cellular uptake in NPCs and present a better therapeutic effect on impaired NPCs.

Modified EVs Restore the Vesicle Uptake of NPCs in a Three-Dimensional Hydrogel. To further investigate the effects of Cavin-2-modified EVs on NPCs, we constructed a 3-D alginate hydrogel *in vitro* culture model, which is close to the living conditions *in vivo* (Figure 6A). TNF- α -impaired NPCs presented different uptake rates of C-EVs and M-EVs around the 3-D culture environment (Figure 6B). Based on the analysis of labeled EV fluorescence intensity, the uptake rates of C-EVs and M-EVs were similar in TNF- α -untreated NPCs.

However, the uptake of C-EVs decreased significantly in TNF- α -treated NPCs compared with that of the M-EVs (Figure 6C). The flow cytometry analysis based on the cells obtained from the 3-D hydrogel also indicated that M-EVs display an improved uptake rate in NPCs compared with the C-EVs (Figure 6D,E). Moreover, we assessed the cell viability of NPCs incubated with EVs in the 3-D hydrogel (Figure 6F). Consistent with the previous results, TNF- α treatment induced the death of NPCs, and the administration of C-EVs or M-EVs could ameliorate the cell death induced by TNF- α . Compared with the C-EVs, the M-EVs presented a lower rate of cell death on TNF- α -treated NPCs (Figure 6G). Collectively, these results showed that M-EVs display a restored vesicle uptake in impaired NPCs and mediated the therapeutic effect in the 3-D hydrogel culture model.

Evaluation of EV-Engineered Therapeutic Effects on an Ex Vivo Disc Culture Model. We then investigated whether the Cavin-2-modified EVs play a role in treating the disc degeneration. In the *ex vivo* disc culture model, the whole disc organ was isolated and cultured in the designed medium, which allows for external additives used at the organ level (Figure 7A). *Ex vivo* imaging showed that C-EVs or M-EVs were retained in the disc for over a week; therefore, we repeated the EV injection procedure weekly (Figure 7B). Degenerated discs were characterized by diminished nucleus pulposus areas and annulus fibrosus with ruptured fibers.³⁰ The hematoxylin and eosin (HE) and Safranin O-fast green (S-O) staining showed the morphology and cell sparsity of nucleus pulposus and annulus fibrosus in the rat disc (Figure 7C,D). Masson staining revealed the ruptured fibers of the annulus fibrosus in the TNF- α -treated disc organ (Figure 7E). These histological staining results indicated that TNF- α led to the degenerative profile of the rat disc, and administration of C-EVs or M-EVs retarded the progression of IDD (Figure 7F). Moreover, M-EVs displayed a better therapeutic effect on IDD compared with the C-EVs. TUNEL analysis results also showed that delivery of C-EVs or M-EVs ameliorated the cell death induced by TNF- α in the *ex vivo* model (Figure 7G). Compared with C-EVs, M-EVs decreased the TNF- α -induced cell death more significantly (Figure 7H). In summary, these data indicated that engineered EVs presented a better therapeutic effect in attenuating disc degeneration in the *ex vivo* model.

CONCLUSIONS

MSC-derived EVs have presented the therapeutic potential in treating the degenerative diseases of intervertebral discs.^{8,9,31} EVs deliver diverse cargoes from MSCs and possess the capacity to trigger phenotypic changes in disc cells. Based on a cell coculture model, we found that MSCs ameliorate the inflammasome activation and pyroptotic cell death in NPCs through their paracrine effect. In a further investigation, we confirmed that EVs from MSCs deliver Prx-2 to regulate inflammasome activation in NPCs. Prx-2 enriched in MSC-EVs protected against cell death of NPCs, while this therapeutic effect weakened in TNF- α -impaired NPCs due to a decreased uptake of EVs. It was indicated that NPCs internalize EVs *via* the caveolae-dependent endocytosis pathway, and Cavin-2 plays a critical role during this process. We then constructed a kind of engineered EV with Cavin-2 expression in the EV membrane, and it could restore the therapeutic effect on NPCs due to the repair of the endocytosis pathway (Figure 8). Moreover, the effects of modified EVs on

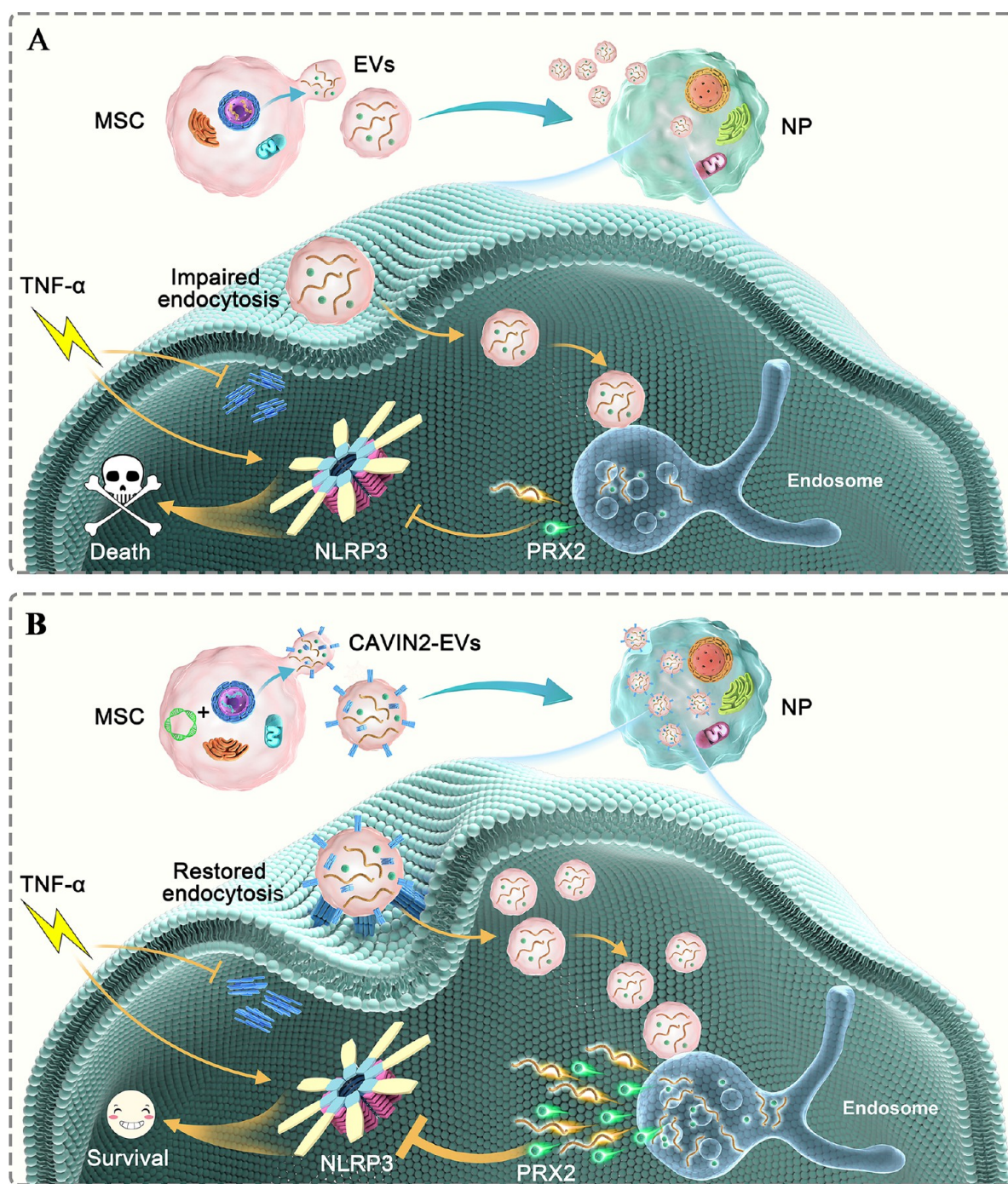


Figure 8. Proposed model for the endocytosis pathway of EVs in NPCs. (A) TNF- α induces the NLRP3 inflammasome activation in NPCs and impairs the endocytosis pathway, which accounts for the decreased therapeutic effect of EVs. Activation of inflammasomes and inflammatory cascades results in cell death ultimately. (B) Engineering EVs produced by Cavin-2-modified MSCs could restore the function of Cavin-2 *via* the caveolae-associated endocytosis pathway. NPCs display a restore uptake rate to Cavin-2-modified EVs. Internalization of Cavin-2-modified EVs plays a therapeutic role in NPCs at inflammatory status and helps NPCs survive upon TNF- α stimulation. EVs, extracellular vesicles; MSC, mesenchymal stem cell; NP, nucleus pulposus; NPCs, nucleus pulposus cells; Cavin-2, caveolae-associated protein 2; PRX2, peroxiredoxin-2; NLRP3, nod-like receptor protein 3; TNF- α , tumor necrosis factor α .

the uptake efficiency and NPCs' viability were evaluated in a 3-D hydrogel cell culture system and an *ex vivo* organ culture model, which could simulate the intercellular environment *in vivo*. Collectively, our study investigated the endocytic mechanism of EVs in NPCs and found that Cavin-2-engineered EVs restored the impaired endocytosis pathway and increased the therapeutic efficacy in regenerating NPCs.

Inflammasome activation with related inflammatory cytokines secretion plays a crucial role in the pathogenesis of IDD.^{32,33} Activated NLRP3 inflammasomes can promote the cleavage of caspase-1, resulting in the maturation and secretion of IL-1 β .³⁴ Accumulation of inflammatory cytokines, such as TNF- α and IL-1 β , and form a harsh microenvironment for disc cells and exacerbate the progression of IDD.^{35,36} The inflammation-related phenotypic changes in disc cells contain

cell senescence, apoptosis, necroptosis, or pyroptosis.³⁷ A recent study proved that GSDMD, a form of programmed inflammatory cell death, could be activated by the NLRP3/caspase-1 axis.¹⁸ The present study also showed that treatment of TNF- α elicits the activation of NLRP3 and caspase-1, as well as the cleavage of GSDMD. The caspase-1 and PI double staining results revealed an increasing rate of pyroptotic cell death in NPCs. Therefore, how to restore the impaired NPCs' function and reduce the cell death may be a primary obstacle for IDD therapy.

Small extracellular vesicles, a kind of cell-free nanosized particles, could serve as an alternative in MSC-based therapy.³⁸ Growing evidence has confirmed the therapeutic effect of MSC-EVs in musculoskeletal diseases, including IDD.⁸ MSC-EVs may prevent excessive apoptosis of NPCs and promote cell proliferation, probably through activation of the pro-survival signaling pathway in recipient cells.^{9,39} Other studies verified the anti-inflammatory property of MSC-EVs, which reduced inflammation and induced a healthier extracellular matrix production in NPCs.⁴⁰ These studies investigated the merit of EVs in IDD therapy, with the premise that disc cells could internalize most exogenous EVs. However, it has to be noted that no studies have investigated whether the functional status of recipient NPCs influences the uptake of EVs. The internalization rate of EVs may directly determine the therapeutic efficiency in NPCs. Our data showed that TNF- α -pretreated NPCs presented a less EV-labeled staining than normal NPCs in the same period of time, which indicated a reduced uptake of EVs in the rate and quantity.

Mechanisms of EV uptake into acceptor cells are still poorly understood. Size or surface molecules of EVs may influence their recognition and internalization by recipient cells.¹¹ Small EVs are mostly likely to be engulfed *via* micropinocytosis, whether involved or not with specific receptors.⁴¹ Recent studies revealed that EVs may be internalized by host cells by clathrin-independent endocytosis, especially caveolae-dependent endocytosis.^{41,42} However, different types of cells may differ in the specific mechanism of EV uptake. On the other hand, proteins localized on the surface of EVs, such as integrins and proteoglycans, play a vital role in the internalization of EVs.⁴³ Research indicated that glycans in the surface of EVs could bind to the cellular chemokine receptor CCR8 *via* a bridging chemokine.⁴⁴ The functional status of recipient cells also could influence the uptake of EVs. Stressed cells could alter the expression of surface ligands and then affect the uptake of exogenous EVs.^{20,21} Since EVs serve as a communication mediator between different cells, the EVs' release and internalization may change in the donor and recipient cells under stressful conditions. Consistent with these studies, our study indicated that impaired cells under inflammatory conditions reduced the uptake of EVs significantly. Therefore, in order to improve the therapeutic potential of MSC-EVs in IDD, it is of great importance to raise the uptake efficiency of EVs in resident disc cells.

Caveolae-dependent endocytosis is a well-known form of clathrin-independent endocytosis, which mediates the internalization of various cargoes.⁴⁵ Caveolae formation mostly relies on caveolin proteins and coated proteins, cavinins.⁴⁶ Cavin proteins, including Cavin-1, Cavin-2, and Cavin-3, are key regulators of caveolae formation and caveolin function.⁴⁷ Among these, Cavin-2 binds to Cavin-1 and induces the formation of membrane curvature.^{28,48} Hansen *et al.* found that loss of Cavin-2 expression caused loss of caveolin-1 and Cavin-

1 expression, while overexpression of Cavin induced the accumulation of plasma membrane curvature.²⁸ Many studies also revealed that Cavin-2 plays roles in cell apoptosis, cancer metastasis, and lipid metabolism, which demonstrated the diverse role of Cavin-2 in cell processes.^{49,50} Our study found that the expression level of Cavin-2 significantly decreased in impaired NPCs, and knockdown of Cavin-2 inhibited the EV uptake, indicating the critical role of Cavin-2 in the NPCs' endocytosis process.

The 3-D cell culture and *ex vivo* disc culture system in our study could simulate the disc condition *in vivo*. For the 3-D hydrogel culture, alginate hydrogel is a hydrophilic and biocompatible material with properties similar to those of the extracellular matrix, which is a reasonable choice for cell culture.^{51,52} These hydrogels could encapsulate cells and form a cellular environment similar to that *in vivo*.⁵³ Moreover, the disc culture with a whole structure of IVDs, including the nucleus pulposus, annulus fibrosus, and adjacent end plates, allows outer substances or nutrients to penetrate, which is a suitable model for disc research.^{54,55} Based on the IVD explants, the *ex vivo* culture system could simulate the *in vivo* status of cells better compared with the *in vitro* studies.⁵⁵ Here, we used the TNF- α to induce the disc degeneration, which is consistent with the results of the *in vitro* studies. The administration of EVs presented a therapeutic effect on disc degeneration and ameliorated the rate of NPC death.

Although the evidence could support our conclusion, there are still some limitations in this study. Compared with siRNA knockdown of Cavin-2, it may be more thorough in gene silencing to use Cavin-2 knockout cell lines. However, there is still no commercial intervertebral disc cell line for laboratory research. Moreover, NPC impairment is induced by TNF- α treatment in our study. There are many inflammatory factors involved in IDD and NPC injury. Therefore, we still need conduct more experiments to confirm our conclusion. Moreover, inflammatory stimulus is involved in the progression of IDD while the initiating factors remain unknown. Inflammatory stimuli may not be responsible for all of the pathogenesis changes of disc cells, and different cell models need to be investigated in a further study.

In conclusion, we demonstrated that EVs effectively protect NPCs from pyroptosis *via* the delivery of peroxiredoxin-2. Our findings also revealed that the therapeutic efficacy of EVs decreased in TNF- α -impaired NPCs due to the inhibition of the endocytosis pathway. We constructed the Cavin-2-modified engineered EVs, which could restore the EV uptake in NPCs. These modified EVs played a role in protecting against cell death in the 3-D hydrogel and the disc organ culture model. Therefore, Cavin-2-modified EVs could serve as a potential therapeutic approach in the treatment of IDD.

METHODS

Cell Culture and Coculture. For NPC isolation, human NP tissues were collected from patients who underwent disc excision surgery. All operations for clinical specimens were accompanied by informed consent from the patients. The NP tissues were cut into pieces enzymatically digested in trypsin (0.25%) for 30 min and then collagenase II (0.2%) for 4 h. Next, they were washed in PBS twice, and the suspension was centrifuged. The sediments were collected and cultured in Dulbecco's modified Eagle medium/nutrient mixture F-12 (DMEM/F-12) containing 15% fetal bovine serum (FBS). The medium was changed twice a week, and NPCs from the second passage were used in our experiments. For MSC isolation, human bone marrow specimens were obtained from the iliac crests of donors.

MSCs were isolated by density gradient centrifugation and adherence to tissue culture plastic. For cell coculture, MSCs from the second passage were cultured in Transwell inserts (Corning, USA) and cocultured with NPCs (at a ratio of NPCs/MSCs = 1:1) seeded in the lower chamber. All cell cultures were maintained in an incubator at 37 °C with 5% CO₂ and 20% O₂. All the experimental protocols were approved by the Ethics Committee of Tongji Medical College, Huazhong University of Science and Technology.

EV Isolation and Identification. Human MSCs were cultured in DMEM/F-12 containing 15% EV-depleted FBS (System Biosciences, USA), and the culture medium was collected. The small EVs were obtained by a differential centrifugation method. Briefly, the medium was centrifuged first at 500g for 10 min, then at 2000g for 30 min, and at 10000g for 1 h. After being filtered through a 0.22 μm filter (Millipore, USA), the remaining supernatant was centrifuged by ultracentrifugation at 110000g (Beckman Type 70 Ti, USA) for 70 min twice. The pellet was suspended in PBS for the further experiments. For morphology analysis, the EVs were fixed with 2.5% glutaraldehyde for 30 min and placed on copper grids. Images were captured by transmission electron microscopy (FEI Tecnai G20 TWIN, USA). The number and size of EVs were assessed by nanoparticle tracking analysis using the NANOSIGHT NS300 system (Malvern, UK).

EV Labeling and Internalization Assay. Purified EVs were labeled with 5 μM PKH26 (Sigma-Aldrich, USA) according to the manufacturer's instructions. In order to remove unincorporated dyes, the mixture was washed in PBS and centrifuged at 110000g for 70 min. For the internalization assay through immunofluorescence analysis, the EVs were suspended in medium and incubated with NPCs at 37 °C. After being the cytoskeleton was stained with phalloidin (Beyotime, China) for 1 h and DAPI (Beyotime, China) for the nucleus for 5 min, NPCs were placed under a fluorescence microscope (Olympus, USA) for image capture. The uptake of EVs was assessed by mean fluorescence intensity of the red fluorescent signal using ImageJ 1.52a (National Institutes of Health, USA). For the internalization assay through flow cytometry, the labeled EVs were incubated with NPCs at 37 °C. Then cells were washed with acid wash buffer to remove the free dyes and washed with PBS twice. After being treated with 0.25% trypsin, the adherent cells were collected and fixed in paraformaldehyde. These cells were then applied to the FACSCalibur flow cytometer (BD Biosciences, USA), and data were analyzed by FlowJo X software (Tree Star, USA).

Cell Viability Evaluation. Cell viability of TNF-α-treated NPCs was assessed by a cell counting kit-8 (CCK-8, Boster, China) according to the standard protocol. NPCs were seeded in a 96-well plate and treated with different doses of TNF-α, and then 10% CCK-8 solution was added into the 96-well plate. After being incubated for 4 h, the samples were measured at 450 nm absorbance using a spectrophotometer (BioTek, Winooski, VT, USA).

Western Blot Analysis. The cells were lysed in RIPA lysis buffer (Beyotime, China). The isolated proteins were separated by sodium dodecyl sulfate polyacrylamide gel electrophoresis and transferred onto a PVDF membrane (Millipore, USA). The membrane was washed in 5% milk for 1 h and then incubated with a primary antibody overnight. The primary antibodies were listed as follows: NLRP3 (Affinity Biosciences, 1:2000), caspase-1 (Proteintech, 1:2000), cleaved caspase-1 (Affinity Biosciences, 1:1000), GSDMD (Proteintech, 1:1000), GSDMD-N (Cell Signaling Technology, 1:1000), Prx2 (Proteintech, 1:4000), Cavin-1 (Proteintech, 1:2000), Cavin-2 (Proteintech, 1:1000), Cavin-3 (Proteintech, 1:500), caveolin-1 (Abcam, 1:10000), caveolin-3 (Abcam, 1:5000), CD63 (Proteintech, 1:1000), Alix (Proteintech, 1:2000), Calnexin (Boster, 1:2000), β-actin (Boster, 1:10000), and GAPDH (Proteintech, 1:50000). After being incubated with horseradish peroxidase (HRP)-conjugated secondary antibodies, the bands were visualized using an ECL plus (Thermo Fisher Scientific, USA). Density of bands in three independent experiments was quantified by ImageJ 1.52a (National Institutes of Health, USA), and the protein levels were normalized to GAPDH or β-actin.

Immunoprecipitation. Whole cell lysates were treated with 50 mM Tris-HCl, 150 mM NaCl, 1 mM EDTA, and 1% NP-40 with a protease inhibitor cocktail (Beyotime, China). The sample (500 μg) at 4 °C was added with 10 μL of anti-caveolin-1 (Abcam, UK) antibody and was incubated overnight with magnetic beads (MCE, China). Then the immunoprecipitates were separated by magnetic adsorption and washed with PBS twice. The magnetic isolated immunoprecipitates were conducted with Western blot assays to detect the expression of caveolin-1 and Cavin-2.

Immunofluorescence Analysis. The cells were fixed with 4% paraformaldehyde for 15 min and permeabilized with 0.2% Triton X-100 for 10 min. After being blocked with 2% goat serum albumin for 1 h, the samples were incubated with a primary antibody overnight. Then, the samples were incubated with fluorescently conjugated secondary antibodies for 1 h in the dark. Nuclei were stained by DAPI (Beyotime, China) for 5 min. For propidium iodide staining, cells were incubated with PI solution (Beyotime, China) for 20 min in the dark. Then samples were washed in PBS to remove unincorporated dyes and then fixed with paraformaldehyde. Images were obtained under a microscope (Olympus, USA) by three independent researchers. The caspase-1 or PI positive cells were quantified by ImageJ 1.52a (National Institutes of Health, USA).

RNA Interfering. Small interfering RNA (siRNA) targeted for PRDX2 or CAVIN2 and scrambled siRNA (si-scr) were synthesized by RiboBio (Guangzhou, China). The sequences were listed as follows: PRDX2-siRNA target for 5'-CACCTAGAAGCT-GAATAGTGACG-3'; CAVIN2-siRNA target for 5'-CACGTCAAATCACCAGAAA-3'. NPCs (5 × 10⁵/well) were seeded and cultured in 24-well plates until 50% confluency, and then transfected siRNA was combined with Lipofectamine 2000 (Invitrogen, USA) according to the manufacturer's protocols. The interfering efficacy in NPCs was detected by Western blot analysis or quantitative real-time polymerase chain reaction (qRT-PCR) at 36 h after transfection. For qRT-PCR, total RNA was extracted and reverse-transcribed and then amplified according to the standard protocols. The primers used were listed as follows: Homo PRDX2, forward 5'-GAAGCTGTCGGACTACAAAAG-3', reverse 5'-TCGGTGGGGCACACAAAAG-3'; Homo CAVIN2, forward 5'-CATCCGGGACAACCTCACAGG-3', reverse 5'-CAGCGTCTAGC-ATGTTCCACCA-3'; Homo GAPDH, forward 5'-TCAAGAAGGTG-GTGAAGCAGG-3', reverse 5'-TCAAAGGTGGAGGAGTGGGT-3'. GAPDH was used for normalization.

RNA Sequencing and Data Analysis. The extraction of RNAs was realized by TRIzol Reagent (Invitrogen, USA) according to the standard protocol. After a primary test for RNA quality and integrity, RNAs were quantified and used for stranded RNA sequencing library preparation. With the help of Seqhealth cooperation (Wuhan, China), the raw sequencing data was enriched and quantified, and then mapped to the human genome using STRA 2.5 software. Differentially expressed (*P* value cutoff of 0.05; fold-change cutoff of 2) genes between groups were identified using edgeR package. For further analysis, Gene ontology (GO) analysis and Kyoto encyclopedia of genes and genomes (KEGG) enrichment analysis for differentially expressed genes were conducted by KOBAS 2.1 software (*P* value < 0.05; FDR < 0.05).

Plasmid Construction and Transfection. Recombinant vector encoding human CAVIN2 (NM_004657) was constructed and subcloned into GV492 lentivirus expression vector by GeneChem Company (Shanghai, China). MSCs were transfected with GV492 empty vector (NC-vector) or GV492-CAVIN2-Lamp2b vector and then selected with puromycin. The expression efficacy in MSCs was assessed by quantitative real time polymerase chain reaction at 48 h after transfection. Cavin-2 overexpressed MSCs were cultured and prepared for EV isolation.

Hydrogel Fabrication and Three-Dimensional Culture. Hydrogels were prepared as follows: a 3% w/v solution of alginate was mixed with a cell suspension containing NPCs and 0.1 M calcium chloride. The mixture was placed onto the slides to form a 2 mm thick hydrogel. For confocal microscopy analysis, the slides were fixed with 4% paraformaldehyde for 15 min. After fixation, the hydrogel was

washed with PBS twice and transferred to a confocal dish, and then images were captured *via* a confocal microscope (Nikon A1R SI Confocal, Japan). For cytometry analysis, the hydrogel was degraded by EDTA and washed by PBS, the cells were then isolated and conducted with cytometry.

Live/Dead Staining. Cell viability of NPCs in 3-D hydrogel was assessed by calcein/PI live/dead assay kit (Beyotime, China) according to the manufacturer's protocol. Briefly, NPCs seeded in hydrogels were collected and washed in PBS to remove the residual medium. Calcein/PI solution was added and incubated with NPCs for 30 min. After being transferred to a confocal dish, images were captured *via* a confocal microscope (Nikon A1R SI Confocal, Japan). The PI positive cells were quantified by ImageJ 1.52a (National Institutes of Health, USA).

IVD Organ Culture Model. IVDs were collected from Sprague–Dawley rats (male, 300 g, 8 weeks old) with the ethical approval of the Animal Experimentation Committee of Huazhong University of Science and Technology. Caudal discs with complete end plates were isolated and cultured in DMEM/F-12 containing 15% FBS and 1% penicillin/streptomycin. The osmolarity of the culture medium was adjusted to 400 mOsm by approximating physiological conditions by the addition of 1.5% of a 5 M NaCl and 0.4 M KCl solution as previously described.⁵⁵ Samples were incubated under a hypoxic atmosphere (37 °C, 5% O₂) with saturated humidity. The discs were treated with or without TNF- α (50 ng/mL), or the discs were injected with EVs (100 μ g/mL, 2 μ L) or PBS (2 μ L) using a 33 gauge needle (Hamilton, Benade, Switzerland). The culture medium was replaced once every 3 days. The injection procedure was repeated weekly in one month.

Ex Vivo Imaging Assay. EVs were labeled with Dil dye (Beyotime, China) according to the manufacturer's protocols. The mixture was washed in PBS and then centrifuged at 110000g for 70 min to remove unincorporated dyes. The labeled EVs (100 μ g/mL, 2 μ L) were injected into the nucleus pulposus area of discs using a 33 gauge needle. At each time point, the *ex vivo* discs were observed on an *in vivo* MS FX PRO imaging system (Bruker, USA). The fluorescence intensity of each disc was then quantified by Bruker MI software (Bruker, USA).

Histological Analysis and TUNEL Staining. The discs were collected 2 weeks or 1 month after the first injection procedure. The samples were fixed in formaldehyde and decalcified slowly and steadily using EDTA (0.5 M, Servicebio, China). After being dehydrated and embedded in paraffin, the paraffin blocks were cut into 4 μ m slices in the coronal plane. These slices were stained with hematoxylin and eosin (HE), Safranin O-fast green (S-O), or Masson solution. The degenerative degree of discs was evaluated by a histological grading scale.²⁷ This scale was based on five categories of disc changes: with 0 points for a normal disc and 15 points for a severely degenerated disc. For TUNEL staining, the slices were deparaffinized and rehydrated and then treated with 0.5% TritonX-100 for 20 min. After being washed with PBS, the slices were incubated with the TUNEL staining kit (Beyotime, China) according to the manufacturer's instructions. Images were captured using a fluorescence microscope (Olympus, BX53, USA), and the positive cells were quantified by ImageJ 1.52a (National Institutes of Health, USA).

Statistical Analysis. Data are presented as the mean \pm standard deviation (SD), and all experiments were performed independently at least in triplicate. Student's *t*-tests were used for comparison between two groups. For multiple group comparisons, one-way or two-way analysis of variance (ANOVA) with Tukey's *post hoc* test was used. Statistical significance was measured using GraphPad Prism 8 software (La Jolla, CA, USA), and a *P* value <0.05 shows a statistical difference (**P* or #*P* < 0.05, ***P* or ##*P* < 0.01, ****P* or ###*P* < 0.001).

ASSOCIATED CONTENT

SI Supporting Information

The Supporting Information is available free of charge at <https://pubs.acs.org/doi/10.1021/acsnano.1c04514>.

Effects of TNF- α on NPCs (Figure S1); quantification results of the Western blot analysis in Figure 1; detection of peroxiredoxin-2 in MSC-derived EVs (Figure S2); immunofluorescence analysis of the internalization of PKH26-labeled EVs in TNF- α -pretreated NPCs (Figure S3); GO and KEGG enrichment analysis of differentially up-expressed genes (Figure S4); Western blot analysis of the caveolae-associated proteins; quantification results of the Western blot analysis in Figure 5 (Figure S5) (PDF)

AUTHOR INFORMATION

Corresponding Authors

Cao Yang – Department of Orthopaedics, Union Hospital, Tongji Medical College, Huazhong University of Science and Technology, Wuhan 430022, China; orcid.org/0000-0002-0058-614X; Email: caoyangunion@hust.edu.cn

Wenbin Hua – Department of Orthopaedics, Union Hospital, Tongji Medical College, Huazhong University of Science and Technology, Wuhan 430022, China; Email: huawb1987@163.com

Shuai Li – Department of Orthopaedics, Union Hospital, Tongji Medical College, Huazhong University of Science and Technology, Wuhan 430022, China; Email: lishuai1818@163.com

Authors

Zhiwei Liao – Department of Orthopaedics, Union Hospital, Tongji Medical College, Huazhong University of Science and Technology, Wuhan 430022, China

Hui Liu – Department of Orthopaedics, Union Hospital, Tongji Medical College, Huazhong University of Science and Technology, Wuhan 430022, China

Liang Ma – Department of Orthopaedics, Union Hospital, Tongji Medical College, Huazhong University of Science and Technology, Wuhan 430022, China

Jie Lei – Department of Orthopaedics, Union Hospital, Tongji Medical College, Huazhong University of Science and Technology, Wuhan 430022, China

Bide Tong – Department of Orthopaedics, Union Hospital, Tongji Medical College, Huazhong University of Science and Technology, Wuhan 430022, China

Gaocai Li – Department of Orthopaedics, Union Hospital, Tongji Medical College, Huazhong University of Science and Technology, Wuhan 430022, China

Wencan Ke – Department of Orthopaedics, Union Hospital, Tongji Medical College, Huazhong University of Science and Technology, Wuhan 430022, China

Kun Wang – Department of Orthopaedics, Union Hospital, Tongji Medical College, Huazhong University of Science and Technology, Wuhan 430022, China

Xiaobo Feng – Department of Orthopaedics, Union Hospital, Tongji Medical College, Huazhong University of Science and Technology, Wuhan 430022, China

Complete contact information is available at: <https://pubs.acs.org/doi/10.1021/acsnano.1c04514>

Author Contributions

[†]Z.L., H.L., and L.M. contributed equally to this work.

Notes

The authors declare no competing financial interest.

ACKNOWLEDGMENTS

This study was supported by the National Natural Science Foundation of China (Grant Nos. 82072505, 81902261, 81904020, 81902260, and 81772401) and the Application Foundation and Advanced Program of Wuhan Science and Technology Bureau (2019020701011457).

REFERENCES

- (1) Clouet, J.; Fusellier, M.; Camus, A.; Le Visage, C.; Guicheux, J. Intervertebral Disc Regeneration: From Cell Therapy to the Development of Novel Bioinspired Endogenous Repair Strategies. *Adv. Drug Delivery Rev.* **2019**, *146*, 306–324.
- (2) Deyo, R.; Mirza, S. Clinical Practice. Herniated Lumbar Intervertebral Disk. *N. Engl. J. Med.* **2016**, *374* (18), 1763–72.
- (3) Priyadarshani, P.; Li, Y.; Yao, L. Advances in Biological Therapy for Nucleus Pulposus Regeneration. *Osteoarthritis Cartilage* **2016**, *24* (2), 206–12.
- (4) Liao, Z.; Wu, X.; Song, Y.; Luo, R.; Yin, H.; Zhan, S.; Li, S.; Wang, K.; Zhang, Y.; Yang, C. Angiopoietin-Like Protein 8 Expression and Association with Extracellular Matrix Metabolism and Inflammation During Intervertebral Disc Degeneration. *J. Cell. Mol. Med.* **2019**, *23* (8), 5737–5750.
- (5) Dowdell, J.; Erwin, M.; Choma, T.; Vaccaro, A.; Iatridis, J.; Cho, S. K. Intervertebral Disk Degeneration and Repair. *Neurosurgery* **2017**, *80* (3s), S46–s54.
- (6) Phinney, D. G.; Pittenger, M. F. Concise Review: Msc-Derived Exosomes for Cell-Free Therapy. *Stem Cells (Durham, NC, U. S.)* **2017**, *35* (4), 851–858.
- (7) Alcaraz, M. J.; Compañ, A.; Guillén, M. I. Extracellular Vesicles from Mesenchymal Stem Cells as Novel Treatments for Musculoskeletal Diseases. *Cells* **2020**, *9* (1), 98.
- (8) Piazza, N.; Dehghani, M.; Gaborski, T. R.; Wuertz-Kozak, K. Therapeutic Potential of Extracellular Vesicles in Degenerative Diseases of the Intervertebral Disc. *Front. Bioeng. Biotechnol.* **2020**, *8*, 311.
- (9) Liao, Z.; Luo, R.; Li, G.; Song, Y.; Zhan, S.; Zhao, K.; Hua, W.; Zhang, Y.; Wu, X.; Yang, C. Exosomes from Mesenchymal Stem Cells Modulate Endoplasmic Reticulum Stress to Protect against Nucleus Pulposus Cell Death and Ameliorate Intervertebral Disc Degeneration *in Vivo*. *Theranostics* **2019**, *9* (14), 4084–4100.
- (10) French, K. C.; Antonyak, M. A.; Cerione, R. A. Extracellular Vesicle Docking at the Cellular Port: Extracellular Vesicle Binding and Uptake. *Semin. Cell Dev. Biol.* **2017**, *67*, 48–55.
- (11) Mathieu, M.; Martin-Jaular, L.; Lavieau, G.; Théry, C. Specificities of Secretion and Uptake of Exosomes and Other Extracellular Vesicles for Cell-to-Cell Communication. *Nat. Cell Biol.* **2019**, *21* (1), 9–17.
- (12) Mulcahy, L. A.; Pink, R. C.; Carter, D. R. Routes and Mechanisms of Extracellular Vesicle Uptake. *J. Extracell. Vesicles* **2014**, *3*, 24641.
- (13) Mercer, J.; Schelhaas, M.; Helenius, A. Virus Entry by Endocytosis. *Annu. Rev. Biochem.* **2010**, *79*, 803–33.
- (14) Mettlen, M.; Chen, P. H.; Srinivasan, S.; Danuser, G.; Schmid, S. L. Regulation of Clathrin-Mediated Endocytosis. *Annu. Rev. Biochem.* **2018**, *87*, 871–896.
- (15) Song, Y.; Wang, Y.; Zhang, Y.; Geng, W.; Liu, W.; Gao, Y.; Li, S.; Wang, K.; Wu, X.; Kang, L.; Yang, C. Advanced Glycation End Products Regulate Anabolic and Catabolic Activities Via Nlrp3-Inflammasome Activation in Human Nucleus Pulposus Cells. *Journal of cellular and molecular medicine* **2017**, *21* (7), 1373–1387.
- (16) Elliott, E. I.; Sutterwala, F. S. Initiation and Perpetuation of Nlrp3 Inflammasome Activation and Assembly. *Immunol. Rev.* **2015**, *265* (1), 35–52.
- (17) de Vasconcelos, N. M.; Lamkanfi, M. Recent Insights on Inflammasomes, Gasdermin Pores, and Pyroptosis. *Cold Spring Harbor Perspect. Biol.* **2020**, *12* (5), a036392.
- (18) He, D.; Zhou, M.; Bai, Z.; Wen, Y.; Shen, J.; Hu, Z. Propionibacterium Acnes Induces Intervertebral Disc Degeneration by Promoting Nucleus Pulposus Cell Pyroptosis Via Nlrp3-Dependent Pathway. *Biochem. Biophys. Res. Commun.* **2020**, *526* (3), 772–779.
- (19) Liao, Z.; Li, S.; Liu, R.; Feng, X.; Shi, Y.; Wang, K.; Li, S.; Zhang, Y.; Wu, X.; Yang, C. Autophagic Degradation of Gasdermin D Protects against Nucleus Pulposus Cell Pyroptosis and Retards Intervertebral Disc Degeneration *in Vivo*. *Oxid. Med. Cell. Longevity* **2021**, *2021*, 5584447.
- (20) Nicholson, C.; Shah, N.; Ishii, M.; Annamalai, B.; Brandon, C.; Rodgers, J.; Nowling, T.; Rohrer, B. Mechanisms of Extracellular Vesicle Uptake in Stressed Retinal Pigment Epithelial Cell Monolayers. *Biochim. Biophys. Acta, Mol. Basis Dis.* **2020**, *1866* (3), 165608.
- (21) Yue, K. Y.; Zhang, P. R.; Zheng, M. H.; Cao, X. L.; Cao, Y.; Zhang, Y. Z.; Zhang, Y. F.; Wu, H. N.; Lu, Z. H.; Liang, L.; Jiang, X. F.; Han, H. Neurons Can Upregulate Cav-1 to Increase Intake of Endothelial Cells-Derived Extracellular Vesicles That Attenuate Apoptosis Via Mir-1290. *Cell Death Dis.* **2019**, *10* (12), 869.
- (22) Yang, S.; Zhang, F.; Ma, J.; Ding, W. Intervertebral Disc Ageing and Degeneration: The Antiapoptotic Effect of Oestrogen. *Ageing Res. Rev.* **2020**, *57*, 100978.
- (23) Meldolesi, J. Exosomes and Ectosomes in Intercellular Communication. *Curr. Biol.* **2018**, *28* (8), R435–R444.
- (24) Lipinski, S.; Pfeuffer, S.; Arnold, P.; Treitz, C.; Aden, K.; Ebsen, H.; Falk-Paulsen, M.; Gisch, N.; Fazio, A.; Kuiper, J.; Luzius, A.; Billmann-Born, S.; Schreiber, S.; Nunez, G.; Beer, H. D.; Strowig, T.; Lamkanfi, M.; Tholey, A.; Rosenstiel, P. Prdx4 Limits Caspase-1 Activation and Restricts Inflammasome-Mediated Signaling by Extracellular Vesicles. *EMBO J.* **2019**, *38* (20), e101266.
- (25) Knoops, B.; Argyropoulou, V.; Becker, S.; Ferté, L.; Kuznetsova, O. Multiple Roles of Peroxiredoxins in Inflammation. *Mol. Cells* **2016**, *39* (1), 60–4.
- (26) Cha, H.; Park, S.; Dan, Y.; Kim, J.; Park, S. Peroxiredoxin2 Deficiency Aggravates Aging-Induced Insulin Resistance and Declines Muscle Strength. *J. Gerontol., Ser. A* **2019**, *74* (2), 147–154.
- (27) Liao, Z.; Li, S.; Lu, S.; Liu, H.; Li, G.; Ma, L.; Luo, R.; Ke, W.; Wang, B.; Xiang, Q.; Song, Y.; Feng, X.; Zhang, Y.; Wu, X.; Hua, W.; Yang, C. Metformin Facilitates Mesenchymal Stem Cell-Derived Extracellular Nanovesicles Release and Optimizes Therapeutic Efficacy in Intervertebral Disc Degeneration. *Biomaterials* **2021**, *274*, 120850.
- (28) Hansen, C. G.; Bright, N. A.; Howard, G.; Nichols, B. J. Sdpr Induces Membrane Curvature and Functions in the Formation of Caveolae. *Nat. Cell Biol.* **2009**, *11* (7), 807–14.
- (29) Li, Z.; Zhou, X.; Gao, X.; Bai, D.; Dong, Y.; Sun, W.; Zhao, L.; Wei, M.; Yang, X.; Yang, G.; Yuan, L. Fusion Protein Engineered Exosomes for Targeted Degradation of Specific Rnas in Lysosomes: A Proof-of-Concept Study. *J. Extracell. Vesicles* **2020**, *9* (1), 1816710.
- (30) Ji, M. L.; Jiang, H.; Zhang, X. J.; Shi, P. L.; Li, C.; Wu, H.; Wu, X. T.; Wang, Y. T.; Wang, C.; Lu, J. Preclinical Development of a MicroRNA-Based Therapy for Intervertebral Disc Degeneration. *Nat. Commun.* **2018**, *9* (1), 5051.
- (31) Xia, C.; Zeng, Z.; Fang, B.; Tao, M.; Gu, C.; Zheng, L.; Wang, Y.; Shi, Y.; Fang, C.; Mei, S.; Chen, Q.; Zhao, J.; Lin, X.; Fan, S.; Jin, Y.; Chen, P. Mesenchymal Stem Cell-Derived Exosomes Ameliorate Intervertebral Disc Degeneration Via Anti-Oxidant and Anti-Inflammatory Effects. *Free Radical Biol. Med.* **2019**, *143*, 1–15.
- (32) Tang, P.; Zhu, R.; Ji, W. P.; Wang, J. Y.; Chen, S.; Fan, S. W.; Hu, Z. J. The Nlrp3/Caspase-1/Interleukin-1 β Axis Is Active in Human Lumbar Cartilaginous Endplate Degeneration. *Clin. Orthop. Relat. Res.* **2016**, *474* (8), 1818–26.
- (33) Tang, P.; Gu, J. M.; Xie, Z. A.; Gu, Y.; Jie, Z. W.; Huang, K. M.; Wang, J. Y.; Fan, S. W.; Jiang, X. S.; Hu, Z. J. Honokiol Alleviates the Degeneration of Intervertebral Disc Via Suppressing the Activation of Txnip-Nlrp3 Inflammasome Signal Pathway. *Free Radical Biol. Med.* **2018**, *120*, 368–379.
- (34) Shi, J.; Zhao, Y.; Wang, K.; Shi, X.; Wang, Y.; Huang, H.; Zhuang, Y.; Cai, T.; Wang, F.; Shao, F. Cleavage of Gsdmd by

Inflammatory Caspases Determines Pyroptotic Cell Death. *Nature* **2015**, *526* (7575), 660–665.

(35) Molinos, M.; Almeida, C. R.; Caldeira, J.; Cunha, C.; Gonçalves, R. M.; Barbosa, M. A. Inflammation in Intervertebral Disc Degeneration and Regeneration. *J. R. Soc., Interface* **2015**, *12* (104), 20141191.

(36) Cunha, C.; Silva, A. J.; Pereira, P.; Vaz, R.; Gonçalves, R. M.; Barbosa, M. A. The Inflammatory Response in the Regression of Lumbar Disc Herniation. *Arthritis Res. Ther.* **2018**, *20* (1), 251.

(37) Zhang, F.; Zhao, X.; Shen, H.; Zhang, C. Molecular Mechanisms of Cell Death in Intervertebral Disc Degeneration (Review). *Int. J. Mol. Med.* **2016**, *37* (6), 1439–48.

(38) Rani, S.; Ryan, A. E.; Griffin, M. D.; Ritter, T. Mesenchymal Stem Cell-Derived Extracellular Vesicles: Toward Cell-Free Therapeutic Applications. *Mol. Ther.* **2015**, *23* (5), 812–823.

(39) Zhang, J.; Zhang, J.; Zhang, Y.; Liu, W.; Ni, W.; Huang, X.; Yuan, J.; Zhao, B.; Xiao, H.; Xue, F. Mesenchymal Stem Cells-Derived Exosomes Ameliorate Intervertebral Disc Degeneration through Inhibiting Pyroptosis. *J. Cell. Mol. Med.* **2020**, *24*, 11742.

(40) Lu, K.; Li, H. Y.; Yang, K.; Wu, J. L.; Cai, X. W.; Zhou, Y.; Li, C. Q. Exosomes as Potential Alternatives to Stem Cell Therapy for Intervertebral Disc Degeneration: *In-Vitro* Study on Exosomes in Interaction of Nucleus Pulposus Cells and Bone Marrow Mesenchymal Stem Cells. *Stem Cell Res. Ther.* **2017**, *8* (1), 108.

(41) Costa Verdera, H.; Gitz-Francois, J. J.; Schiffelers, R. M.; Vader, P. Cellular Uptake of Extracellular Vesicles Is Mediated by Clathrin-Independent Endocytosis and Macropinocytosis. *J. Controlled Release* **2017**, *266*, 100–108.

(42) Rai, A. K.; Johnson, P. J. *Trichomonas Vaginalis* Extracellular Vesicles are Internalized by Host Cells Using Proteoglycans and Caveolin-Dependent Endocytosis. *Proc. Natl. Acad. Sci. U. S. A.* **2019**, *116* (43), 21354–21360.

(43) Fuentes, P.; Sese, M.; Guijarro, P. J.; Emperador, M.; Sanchez-Redondo, S.; Peinado, H.; Hummer, S.; Cajal, S. R. Itgb3-Mediated Uptake of Small Extracellular Vesicles Facilitates Intercellular Communication in Breast Cancer Cells. *Nat. Commun.* **2020**, *11* (1), 4261.

(44) Berenguer, J.; Lagerweij, T.; Zhao, X. W.; Dusoswa, S.; van der Stoop, P.; Westerman, B.; de Gooijer, M. C.; Zoetemelk, M.; Zomer, A.; Crommentuijn, M. H. W.; Wedekind, L. E.; Lopez-Lopez, A.; Giovanazzi, A.; Bruch-Oms, M.; van der Meulen-Muileman, I. H.; Reijmers, R. M.; van Kuppevelt, T. H.; Garcia-Vallejo, J. J.; van Kooyk, Y.; Tannous, B. A.; et al. Glycosylated Extracellular Vesicles Released by Glioblastoma Cells are Decorated by Ccl18 Allowing for Cellular Uptake Via Chemokine Receptor Ccr8. *J. Extracell. Vesicles* **2018**, *7* (1), 1446660.

(45) Ferreira, A. P. A.; Boucrot, E. Mechanisms of Carrier Formation During Clathrin-Independent Endocytosis. *Trends Cell Biol.* **2018**, *28* (3), 188–200.

(46) de Almeida, C. J. G. Caveolin-1 and Caveolin-2 Can Be Antagonistic Partners in Inflammation and Beyond. *Front. Immunol.* **2017**, *8*, 1530.

(47) Nassar, Z. D.; Parat, M. O. Cavin Family: New Players in the Biology of Caveolae. *Int. Rev. Cell Mol. Biol.* **2015**, *320*, 235–305.

(48) Parton, R. G.; Tillu, V. A.; Collins, B. M. Caveolae. *Curr. Biol.* **2018**, *28* (8), R402–R405.

(49) Ozturk, S.; Papageorgis, P.; Wong, C. K.; Lambert, A. W.; Abdolmaleky, H. M.; Thiagalingam, A.; Cohen, H. T.; Thiagalingam, S. Sdpr Functions as a Metastasis Suppressor in Breast Cancer by Promoting Apoptosis. *Proc. Natl. Acad. Sci. U. S. A.* **2016**, *113* (3), 638–43.

(50) Hansson, B.; Rippe, C.; Kotowska, D.; Wasserstrom, S.; Sall, J.; Goransson, O.; Sward, K.; Stenkula, K. G. Rosiglitazone Drives Cavin-2/Sdpr Expression in Adipocytes in a Cebpalpha-Dependent Manner. *PLoS One* **2017**, *12* (3), e0173412.

(51) Łabowska, M. B.; Cierluk, K.; Jankowska, A. M.; Kulbacka, J.; Detyna, J.; Michalak, I. A Review on the Adaption of Alginate-Gelatin Hydrogels for 3D Cultures and Bioprinting. *Materials* **2021**, *14* (4), 858.

(52) Gonzalez-Pujana, A.; Vining, K. H.; Zhang, D. K. Y.; Santos-Vizcaino, E.; Igartua, M.; Hernandez, R. M.; Mooney, D. J. Multifunctional Biomimetic Hydrogel Systems to Boost the Immunomodulatory Potential of Mesenchymal Stromal Cells. *Biomaterials* **2020**, *257*, 120266.

(53) Pozzi, S.; Scomparin, A.; Israeli Dangoor, S.; Rodriguez Ajamil, D.; Ofek, P.; Neufeld, L.; Krivitsky, A.; Vaskovich-Koubi, D.; Kleiner, R.; Dey, P.; Koshrovski-Michael, S.; Reisman, N.; Satchi-Fainaro, R. Meet Me Halfway: Are *in Vitro* 3D Cancer Models on the Way to Replace *in Vivo* Models for Nanomedicine Development? *Adv. Drug Delivery Rev.* **2021**, *175*, 113760.

(54) Teixeira, G. Q.; Leite Pereira, C.; Castro, F.; Ferreira, J. R.; Gomez-Lazaro, M.; Aguiar, P.; Barbosa, M. A.; Neidlinger-Wilke, C.; Goncalves, R. M. Anti-Inflammatory Chitosan/Poly- Γ -Glutamic Acid Nanoparticles Control Inflammation While Remodeling Extracellular Matrix in Degenerated Intervertebral Disc. *Acta Biomater.* **2016**, *42*, 168–179.

(55) Wu, X.; Liao, Z.; Wang, K.; Hua, W.; Liu, X.; Song, Y.; Zhang, Y.; Yang, S.; Yang, C. Targeting the Il-1 β /Il-1ra Pathways for the Aggregation of Human Islet Amyloid Polypeptide in an *ex Vivo* Organ Culture System of the Intervertebral Disc. *Exp. Mol. Med.* **2019**, *51* (9), 1–16.